Journal of Magnetism and Magnetic Materials 605 (2024) 172357

Contents lists available at ScienceDirect

Journal of Magnetism and Magnetic Materials

journal homepage: www.elsevier.com/locate/jmmm

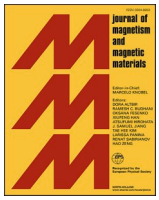

Theoretical perspectives on the electronic, optical, mechanical, magnetic, and anisotropic behaviors of the quaternary Heusler alloys RhFeMnZ and IrMnCrZ (where Z = Si, Ge)

H. Baaziz [a,b,*], T. Ghellab [a,b], Z. Charifi [a,b]

[a] Department of Physics, Faculty of Science, University of M'sila, 28000 M'sila, Algeria
[b] Laboratory of Physics and Chemistry of Materials, University of M'sila, Algeria

ARTICLE INFO

Keywords:
Half-metallicity
Optical response
Spintronic devices
Optoelectronics

ABSTRACT

High-spin-polarised materials are the most promising candidates for spintronic devices. Here, the spin-polarised electronic structure, magnetism, mechanical, and optical properties of RhFeMnZ and IrMnCrZ (where Z = Si, Ge) Quaternary Heusler alloys were calculated by first-principles calculations. The calculations show that type III for the RhFeMnSi, RhFeMnGe, and IrMnCrSi and type I for the IrMnCrGe compound configuration is the most stable crystal structure for the studied alloys. The four alloys were found to have a half-metallic ferromagnetic structure with indirect band gaps in the majority spin channels of 0.957, 0.66, 0.745, and 0.891 eV for RhFeMnSi, RhFeMnGe, IrMnCrSi, and IrMnCrGe, respectively. They exhibit an appreciable total magnetic moment of 4 μ_B for RhFeMnZ (Z = Si, Ge) and 2 μ_B for IrMnCrZ (Z = Si, Ge). The results show that RhFeMnZ and IrMnCrZ (where Z = Si, Ge) are ferromagnetic half-metals with 100 % spin polarisation. The results of the elastic constants demonstrate the mechanical stability of RhFeMnZ and IrMnCrZ (where Z = Si, Ge) alloys. Optical properties such as dielectric function, absorption, reflectance, optical conductivity, and other optical properties were also probed. In the ultraviolet region, RhFeMnZ and IrMnCrZ (where Z = Si, Ge) are effective absorbers and have a high refractive index. Alloys are promising candidates for potential applications in spintronic devices.

1. Introduction

The scientific community has shown increasing interest in the study of Heusler alloys since the theoretical discovery of the first half-metallic (HM) NiMnSb alloy by de-Groot in 1983 [1]. These materials are utilized in spintronics and magnetoelectronics applications [2–8], due to their unique and intriguing structural and magnetic properties. Electrons in one spin channel of these materials demonstrate metallic behavior, while in the other spin channel they exhibit either semiconducting or insulating behavior. The spin polarization is 100 %, and the electronic structure can be adjusted. These materials also have a high Curie temperature [9–11].

Multiple empirical and theoretical research have shown that the quaternary Heusler alloys (EQH) CoFeMnSi alloy has a semi-metallic characteristic [12]. Gao *et al.* [13] established theoretical predictions stating that the EQH alloys CoFeCrAl and CoFeCrSi display complete semi-metallic properties, while CoFeCrGa and CoFeCrGe exhibit almost semi-metallic qualities. In their research, Berri *et al.* [14] studied the electronic and magnetic properties of the CoFeTiSb alloy, known as EQH. They made a prediction that this alloy exhibits a ferromagnetic semi-metallic behavior. Gao *et al.* and Wang *et al.* [15,16] conducted research on Zr-based EQH alloys. Through the use of first principles, they discovered that these alloys are spin-gap-free semiconductors. Moreover, they concluded that Zr-based EQH alloys hold significant potential for applications in spintronics. In their study, Wang *et al.* [17] conducted a thorough analysis of the impact of uniform deformation on the semi-metallic characteristics of FeMnCrZ quaternary HeuslerGG alloys, where Z represents elements such as P, As, Sb, Bi, Se, and Te. In their experimental investigation, Jin *et al.* [18] examined the cubic phase of CoFeCrSi and CoFeCrGe and found that CoFeCrSi exhibits high thermal stability, but CoFeCrGe undergoes disintegration into new compounds at a temperature of 675 K. Bainsla *et al.* [19] experimentally determined that the Curie temperature of CoFeMnGe is around 750 K, and no additional phase transformation occurs up to the melting point. Furthermore, the spin polarization value of 0.67 ± 0.02 in CoFeCrAl is determined using point-contact Andreev reaction measurements [20].

* Corresponding author at: Department of Physics, Faculty of Science, University of M'sila, 28000 M'sila, Algeria.
E-mail address: hakim.baaziz@univ-msila.dz (H. Baaziz).

https://doi.org/10.1016/j.jmmm.2024.172357
Received 17 December 2023; Received in revised form 13 May 2024; Accepted 17 July 2024
Available online 20 July 2024

Table 1
Heusler's three crystalline structure types for the quaternary compounds.

Type	4a (0, 0, 0)	4c (1/4, 1/4, 1/4)	4b (1/2, 1/2, 1/2)	4d (3/4, 3/4, 3/4)
Y-Type I	X=(Rh; Ir)	X_0=(Fe; Mn)	Z=(Ge; Si)	Y=(Mn; Cr)
Y-Type II	X=(Rh; Ir)	Z=(Ge; Si)	X_0=(Fe; Mn)	Y=(Mn; Cr)
Y-Type III	X_0=(Fe; Mn)	Z=(Ge; Si)	X=(Rh; Ir)	Y=(Mn; Cr)

Previous research [12–20] motivated us to conduct a more in-depth analysis of the structural, electronic, magnetic, and optical characteristics of the quaternary Heusler compounds RhFeMnZ and IrMnCrZ (Z = Si, Ge).

Quaternary Heusler alloys, specifically RhFeMnZ and IrMnCrZ (where Z represents Si, Ge), have garnered significant attention due to their unique electronic, magnetic, and structural characteristics, according to research by Nepal *et al.* [21]. These alloys provide a blend of advantageous characteristics, rendering them highly viable contenders for a range of applications, such as photovoltaic cells, optical fibers, thermoelectric modules, and spintronic sensors. The Heusler crystal structure, found in RhFeMnZ and IrMnCrZ alloys, is responsible for determining their structural properties. This crystal structure is typically composed of two face-centered cubic sublattices that interpenetrate each other. This arrangement enables the creation of a diverse array of stable compositions with adjustable lattice parameters, enabling customization of material properties. From an electrical standpoint, these alloys exhibit intricate band structures with various characteristics, such as spin-polarized bands, half-metallic properties, or semiconducting behavior. These traits are determined by the exact composition of the alloy and the selection of the Z element. Using first-principles calculations, the structural, electronic, mechanical, magnetic and optical features of these novel compounds RhFeMnZ and IrMnCrZ (Z = Si, Ge) are investigated. As per the literature survey, neither experimental nor theoretical investigations have been conducted on these compounds, which motivated us to initiate studies on them. To achieve this, we employed first-principles calculations based on density functional theory (DFT) using the linearized augmented plane wave method (LAPW) with a total potential implemented in the WIEN2k code. The generalized gradient approximation (GGA) is employed to compute the total energy by considering the exchange–correlation potential. Furthermore, the modified Beck-Johnson (mBJ) method is employed to compute electronic, magnetic, and optical characteristics.

2. Computational details and methodology

We have used the FP-LAPW method [22] based on DFT [23] as implemented in WIEN2k code [24] to predict the electronic structure results of RhFeMnZ and IrMnCrZ (Z = Si, and Ge). Both materials crystallize in the space group of (#216), having minimum energy in the ferromagnetic (FM) state. Optimization of the magnetic ground state was achieved by applying the generalized gradient approximation (GGA) method of Perdew, Burke, and Ernzerhof (PBE) [25]. The energy-volume (E-V) data obtained from the code was fitted via Birch Murnaghan's equation of state [26]. The maximum limit of the angular momentum vector (l_{max}) was set at 10, while the upper limit of the Fourier expansion of charge density (G_{max}) was selected at 12, and the product RMT × k_{max} = 8.0. The RMT values for Rh, Fe, Mn, Ir, Cr, Si, and Ge are 2.24, 2.24, 2.24, 2.32, 2.20, 1.86, and 2.15 a.u. for both RhFeMnZ and IrMnCrZ (Z = Si, and Ge). The energy and charge convergence were considered within 0.0001 Ry and 0.001 $a.u.^3$ per unit cell. Calculations are carried out in a k-mesh of 1000 k points in an irreducible Brillouin zone using the tetrahedron method [27]. The further Charpin method [28], as implemented in WIEN2k code, was used to compute elastic constant data for all compounds.

3. Results and discussion

3.1. Crystal structure, morphology and stability

Compounds belonging to the Heusler quaternary group are characterized by a unit cell comprising four distinct elements and a space group of (#216). XX_0YZ is the chemical formula, where Y is a metalloid atom and X, X_0, and Y are transition metal atoms. Stable structures are typically those in which atom X possesses a greater number of valence electrons than atoms X_0 and Y, while atom Y has a smaller number of valence electrons than atom X_0 [29]. As shown in Table 1, quaternary Heusler compounds have the potential to crystallize into one of three distinct crystal structures, specifically Y-type structures. Fig. 1 illustrates the crystal structures of the compounds RhFeMnZ and IrMnCrZ (Z = Si, and Ge). In order to determine the most stable type among the three types for each compound in the magnetic (Ferromagnetic) and non-magnetic (Paramagnetic) states, the energy contours must be plotted according to Fig. 2. In Table 2, we have also presented comparisons between the theoretical results available in the literature and our findings regarding lattice parameter *a*, and the compressibility modulus for each of the compounds RhFeMnZ and IrMnCrZ (Z = Si, and Ge). As shown in Table 1, the quaternary Heusler materials RhFeMnZ and IrMnCrZ (Z = Si, Ge) may possess one of three possible structures. Consequently, ground-state energies were evaluated and every type was investigated.

Ferromagnetic states are among the configurations that quaternary Heusler compounds can assume. The compounds RhFeMnSi, RhFeMnGe, and IrMnCrSi are classified as type III, whereas the IrMnCrGe compound is classified as type I. Table 2 presents the optimized lattice parameters, which exhibit a high degree of concordance with findings from other theoretical investigations [21]. The lattice parameter optimized for the quaternary Heusler compounds RhFeMnZ and IrMnCrZ (where Z represents Si, Ge) is in excellent concurrence with the theoretical value documented by Nepal *et al.* [21]. The IrMnCrSi

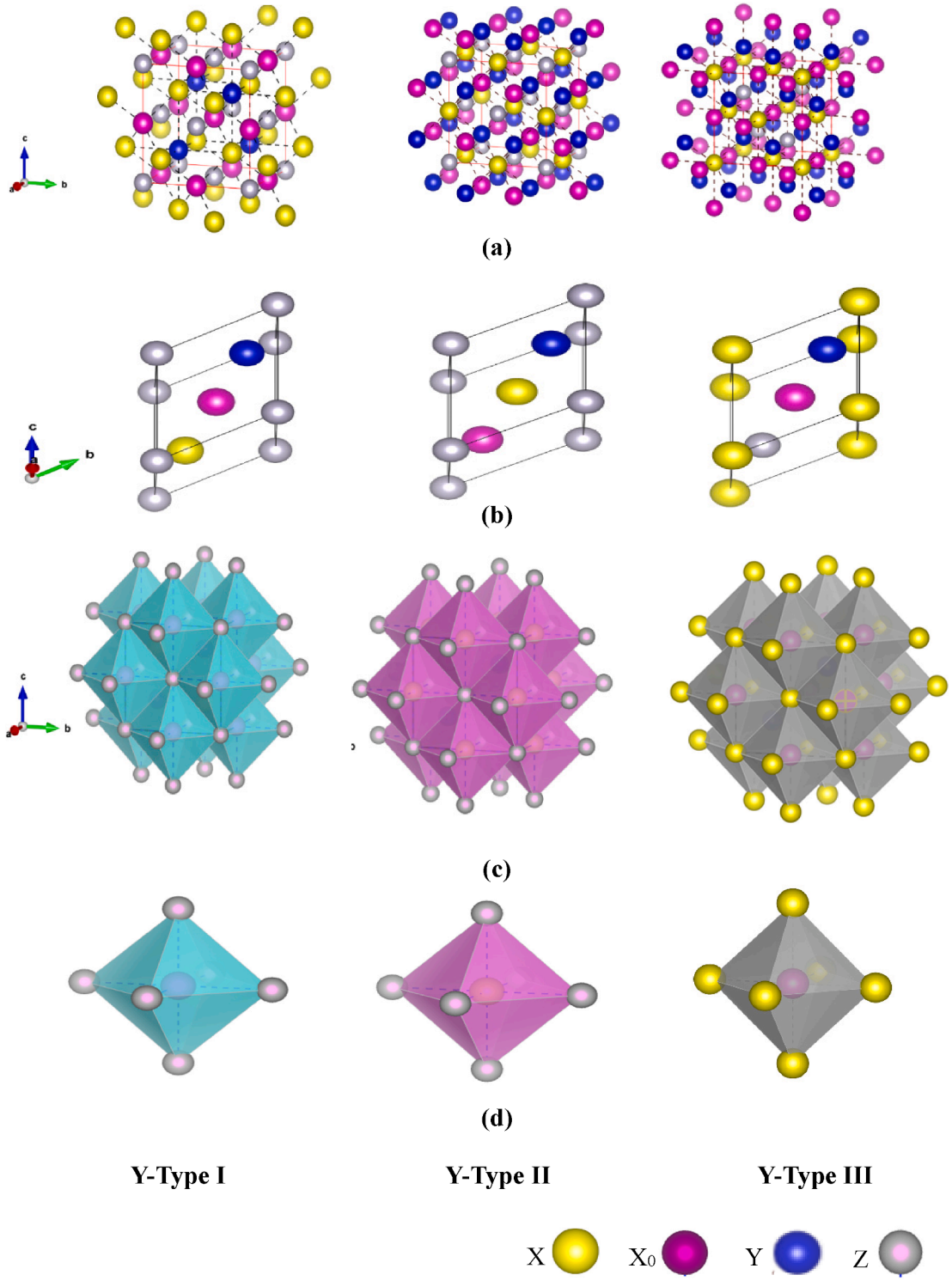

Fig. 1. The three different cell types (a) conventional along the (1 1 1) direction, (b) primitive along the ($\bar{1}$11) direction (c) octahedral configurations along the (1 1 1) direction, and (d) X0Z6, XZ6, X0X6 octahedra along the (1 1 1) direction, of XX_0YZ quaternary compounds.

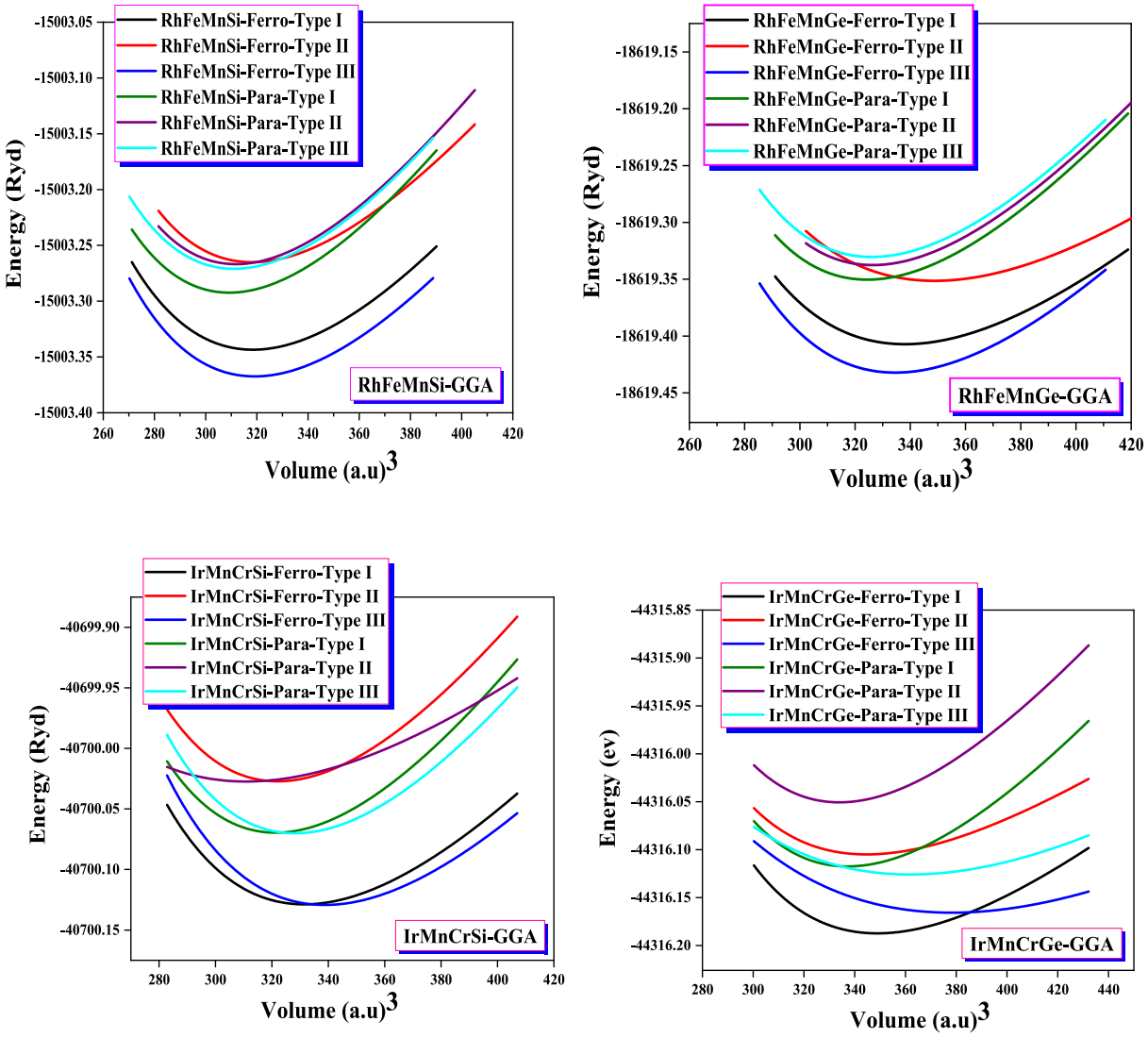

Fig. 2. The variation of energy as a function of volume in the three types in the magnetic and non-magnetic case of the Heusler quaternary compounds RhFeMnZ and IrMnCrZ (where Z = Si; Ge).

compound exhibits the highest modulus of compressibility in its ferromagnetic phase, followed by RhFeMnSi, IrMnCrGe, and RhFeMnGe. To the best of our knowledge, there are currently no published data regarding the compressibility modulus data of these intriguing compounds.

Cohesive and formation energies can be utilized to determine the physicochemical stability of quaternary RhFeMnZ and IrMnCrZ (where Z represents Si, and Ge) Heusler alloys:

$$E_{coh} = \frac{1}{4}\left[E_{Tot}^{XX_0YZ} - \left(E_{atom}^{X} + E_{atom}^{X_0} + E_{atom}^{Y} + E_{atom}^{Z}\right)\right] \quad (1)$$

$$E_{For} = \frac{1}{4}\left[E_{Tot}^{XX_0YZ} - \left(E_{bulk}^{X} + E_{bulk}^{X_0} + E_{bulk}^{Y} + E_{bulk}^{Z}\right)\right] \quad (2)$$

where $E_{Tot}^{XX_0YZ}$ is the equilibrium total energy in the most stable phase for RhFeMnZ and IrMnCrZ (where Z represents Si, and Ge). E_{atom}^{X}, $E_{atom}^{X_0}$, E_{atom}^{Y}, and E_{atom}^{Z} are the isolated atomic energies of the elements X = Rh/Ir, X_0 = Fe/Mn, Y = Mn/Cr, and Z = Si/Ge, for RhFeMnZ/IrMnCrZ (Z = Si, Ge), respectively, E_{bulk}^{X}, $E_{bulk}^{X_0}$, E_{bulk}^{Y}, and E_{bulk}^{Z} are the equilibrium total energies per atom for bulk X = Rh/Ir, X_0 = Fe/Mn, Y = Mn/Cr, and Z = Si/Ge, for RhFeMnZ/IrMnCrZ (Z = Si, Ge), respectively. The formation /

Table 2
The estimated lattice constant *a*, the compressibility module *B* calculated by GGA approximation of the quaternary Heusler compounds: RhFeMnSi, RhFeMnGe, IrMnCrSi, and IrMnCrGe.

Compounds	The types	Parameters	Our calculations		Other calculations [21]
			Para	Ferro	
RhFeMnSi	Type I	*a* (Å)	5.6812	5.7367	5.8088
		B (GPa)	272.9219	243.3475	–
	Type II	*a* (Å)	5.6970	5.7357	5.8821
		B (GPa)	270.9099	246.5291	–
	Type III	*a* (Å)	5.6923	5.7408	5.8021
		B (GPa)	268.9799	247.8967	–
RhFeMnGe	Type I	*a* (Å)	5.7730	5.8522	5.9475
		B (GPa)	260.5828	195.3703	–
	Type II	*a* (Å)	5.7836	5.9135	6.0225
		B (GPa)	256.8395	157.0286	–
	Type III	*a* (Å)	5.7826	5.8320	5.9089
		B (GPa)	257.1644	230.3151	–
IrMnCrSi	Type I	*a* (Å)	5.7543	5.8140	5.8909
		B (GPa)	288.7840	239.8292	–
	Type II	*a* (Å)	4.7055	5.2779	–
		B (GPa)	5.7788	5.7790	5.9115
	Type III	*a* (Å)	282.3439	276.0708	–
		B (GPa)	5.7531	5.8138	5.8485
IrMnCrGe	Type I	*a* (Å)	5.8476	5.9146	6.0098
		B (GPa)	268.4090	214.4218	–
	Type II	*a* (Å)	5.8603	5.9223	6.0425
		B (GPa)	265.0354	174.3036	–
	Type III	*a* (Å)	5.8418	5.8771	5.9509
		B (GPa)	269.9556	245.6076	–

cohesion energies for RhFeMnSi, RhFeMnGe, IrMnCrSi, and IrMnCrGe have been calculated to be −0.56/-6.18 eV/atom, −0.38/-5.79 eV/atom, −0.53/-6.53 eV/atom and −0.32/-6.12 eV/atom, respectively. The negative numbers demonstrate the stability and feasibility of the experimental synthesis of these four materials. Due to its minimal formation energy, RhFeMnSi exhibits the highest simplicity in synthesis. As a consequence of these findings, additional examinations were carried out exclusively on the structure of RhFeMnZ and IrMnCrZ (where Z represents Si, Ge) with regard to their electronic, elastic, and magnetic properties.

3.2. Elastic properties, mechanical stability and mechanical aspects

A comprehensive understanding of solid elasticity is essential for grasping their mechanical characteristics and maximising their worth in diverse sectors and technological applications. The solid is capable of regaining its initial state subsequent to deformation. since the procedure itself is reversible, especially when subjected to small deformations that adhere to linear elasticity principles and exhibit linear stress–strain correlations. Nevertheless, when materials encounter significant deformations, they can experience irreversible alterations. “Permanent

Table 3
The elastic parameters, the anisotropy index, the melting temperature T_{melt}, the velocity of both the longitudinal and transverse waves ($\boldsymbol{v_t}$, $\boldsymbol{v_l}$), the mean velocity of sound ($\boldsymbol{v_m}$), and the temperature of Debye Θ_D.of the quaternary Heusler compounds IrMnCrGe-Type I IrMnCrSi-Type III, RhFeMnGe-Type III, and RhFeMnSi-Type III.

	IrMnCrGe-Type I	IrMnCrSi-Type III	RhFeMnGe-Type III	RhFeMnSi-Type III
C_{11} (GPA)	289.4194	340.5085	307.8988	347.7091
C_{12} (GPA)	179.3887	192.7233	193.3665	200.3257
C_{44} (GPA)	151.0978	170.2879	144.2741	162.9908
B_H (GPA)	216.065	241.985	231.544	249.453
G_V (GPA)	112.664	131.729	109.470	127.270
G_R (GPA)	88.955	111.898	89.736	109.778
G_H (GPA)	100.809	121.813	99.603	118.524
E_V (GPA)	287.943	334.491	283.700	326.315
E_R (GPA)	234.661	290.860	238.409	287.203
E_H (GPA)	261.723	312.930	261.336	306.956
σ_V	0. 277	0. 269	0.295	0. 281
σ_R	0. 318	0. 299	0.328	0. 308
σ_H	0. 298	0. 284	0. 311	0. 294
A_1	2.74647	2.30453	2.51936	2.21179
T_{melt} (K)	2263.468 ± 300	2565.405 ± 300	2372.681 ± 300	2607.960 ± 300
B_H/G_H	1.55745	1.98651	2.32465	2.10465
A_G %	11.7597	8.14018	9.90621	7.37909
A^U	1.33268	0.886152	1.09954	0.796698
v_t (m/s)	2906.23	3318.55	3223.09	3736.79
v_l (m/s)	5418.89	6046.55	6164.45	6928.7
v_m (m/s)	3245.42	3699.54	3605.59	4171.23
Θ_D (K)	411.653	477.39	463.815	545.102

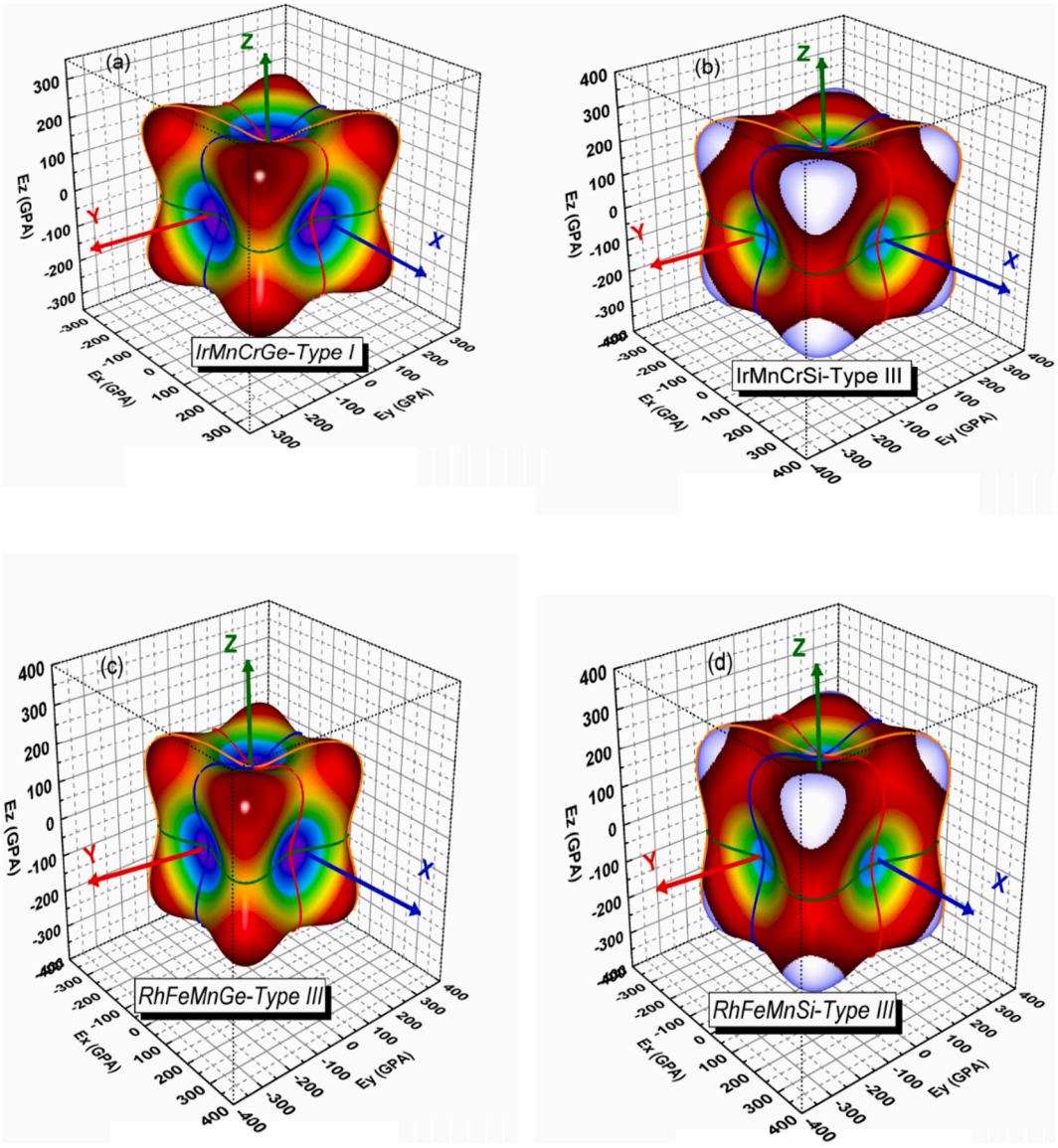

Fig. 3. Young's modulus surfaces in 3D for **(a)** IrMnCrGe, **(b)** IrMnCrSi, **(c)** RhFeMnGe and **(d)** RhFeMnSi and **(e)**, **(f)**, **(g)** and **(h)** their respective cross-section in different planes.

changes" denote alterations or variations in the structure or characteristics of a material that endure even in the absence of the deforming source or pressure. These changes represent a permanent transformation in the substance's condition and cannot be undone. Practically, this could involve alterations in the form, dimensions, or mechanical characteristics of a material. These alterations endure even in the absence of external forces or deformations acting upon the material. The elastic constants of RhFeMnZ and IrMnCrZ (Z = Si, Ge) materials are obtained using density functional theory (DFT) in first computational assessments. This entails precisely inducing a state of minimal stress in the material's structure. The cubic elastic package, integrated into WIEN2k, has been utilised for this particular objective [30]. In cubic systems, just three independent second-order elastic parameters are required: C_{11}, C_{12}, and C_{44}. These metrics are used to determine the material's

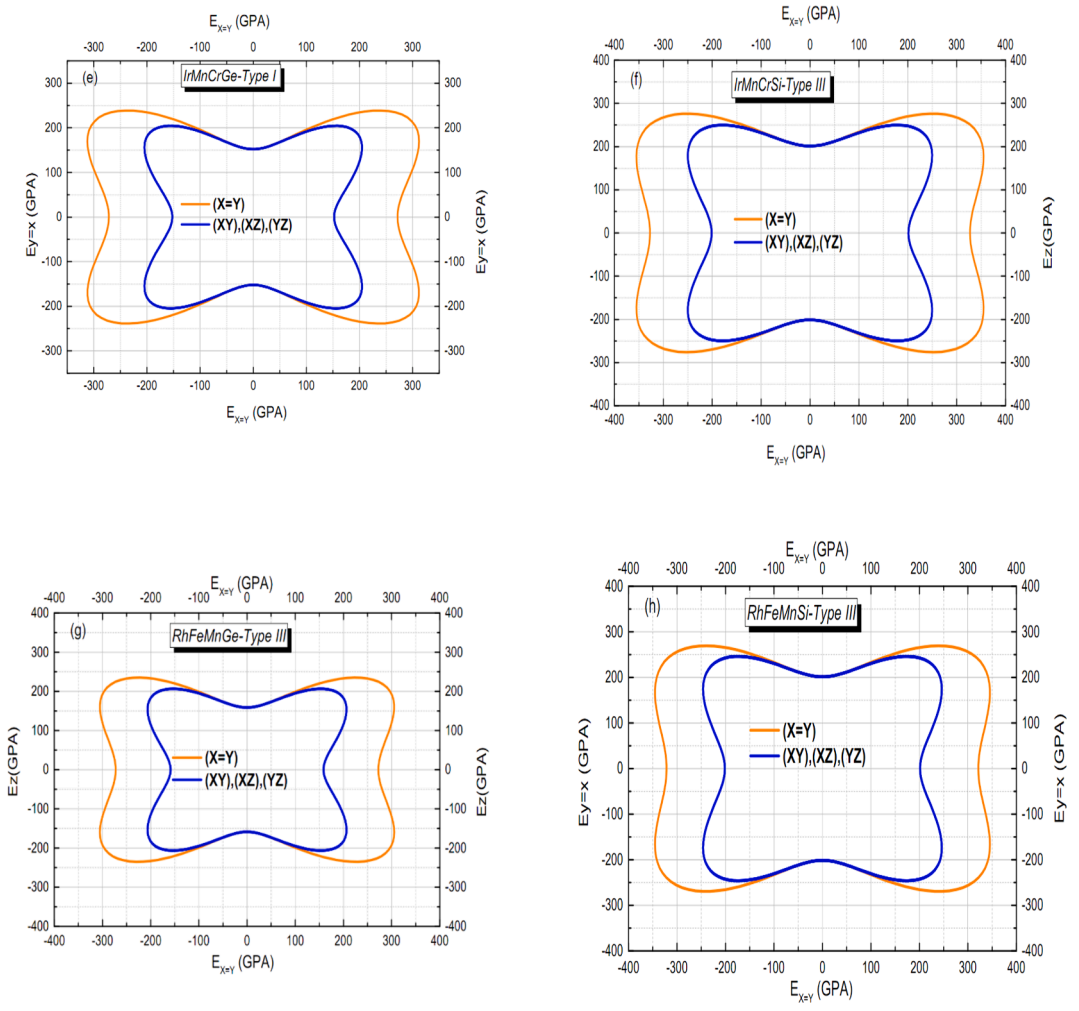

Fig. 3. (*continued*).

resilience. C_{11} represents the state of being compressed in the direction of the length and is related to the hardness of the material. C_{12} elucidates the characteristics of transverse deformation, which is intricately linked to the ratio of Poisson. The shear modulus is specified by the C_{44}. The calculations yielded results presented in Table 3, which clearly show that each of the C_{ij} values measured in GPa, was positive. This substantiates the compounds' undeniable capacity to maintain their shape under pressure, and it aligns with the stability requirements proposed by the generalised Born Huang conditions [31,32]. Based on the above conditions for the elastic tensor:

$$C_{11} - C_{12} > 0, C_{11} > 0, C_{44} > 0, C_{11} + 2C_{12} > 0, C_{11} < B < C_{12} \quad (3)$$

Computational methods can be used to calculate several comprehensive elastic moduli, including the bulk modulus (B), Young's modulus (E), and shear modulus (G). The bulk modulus measures the resistance of a substance to changes in volume caused by external pressure. The Young's modulus quantifies the resistance of a material to deformation when subjected to axial or tensile stress. As an alternative name for the modulus of rigidity, the shear modulus quantifies the resistance of a material to shear deformation. The ductility or brittleness of a material can be assessed by examining various parameters, including the Pugh ratio (B/G), Poisson's ratio (σ), Zener's anisotropy ($A_1 = \frac{2C_{44}}{C_{11}-C_{12}}$), and Cauchy's pressure ($C_p = C_{12}$-C_{44}). When we compare the calculated bulk modulus values of RhFeMnZ and IrMnCrZ (where Z = Si, Ge), we find that there is a significant separation. There is a clear difference in the volume shift between RhFeMnZ and IrMnCrZ (Z = Si, and Ge),

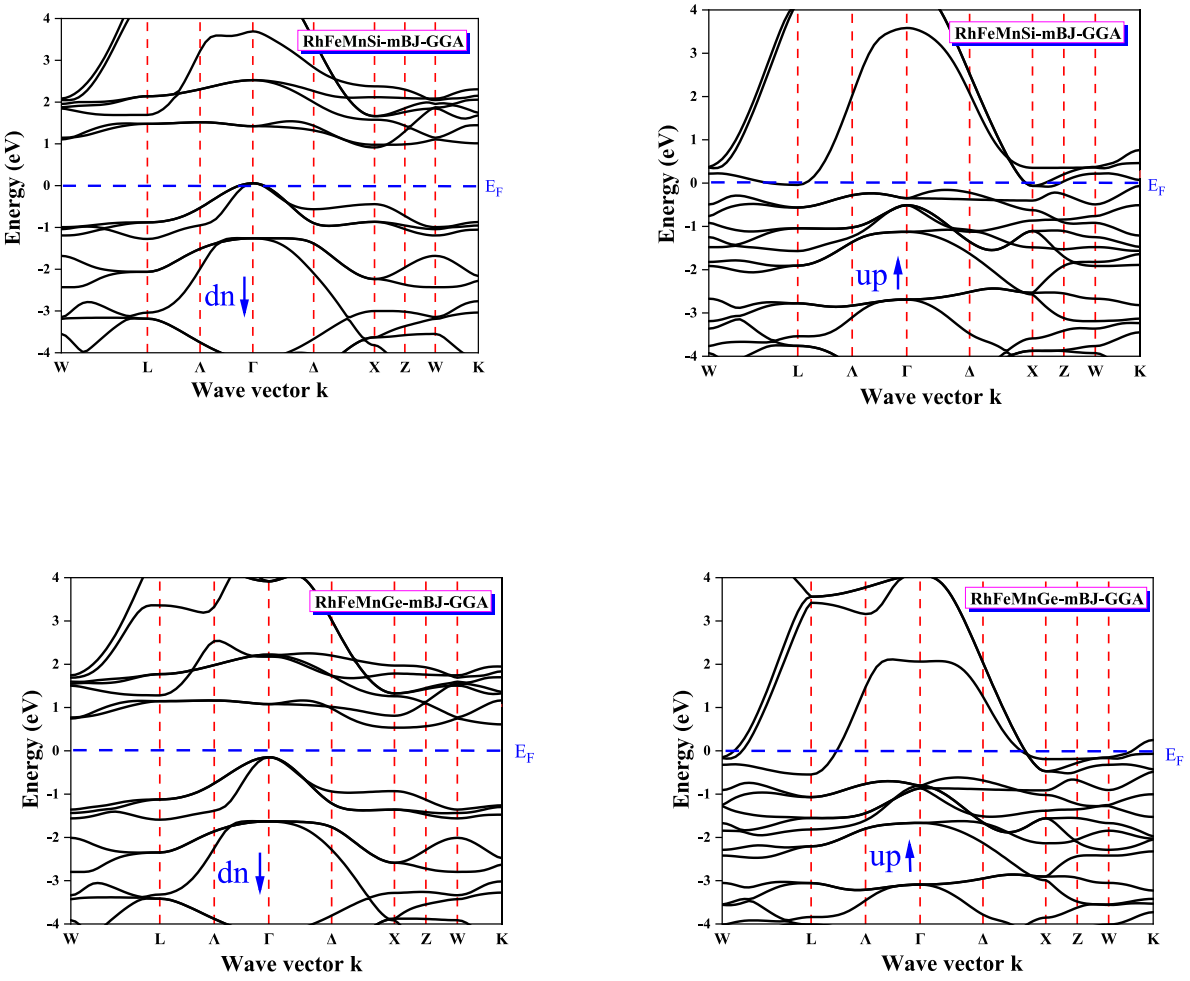

Fig. 4. Calculation of the Heusler quaternary compounds RhFeMnZ and IrMnCrZ (where Z = Si; Ge) band structure using mBJ-GGA.

suggesting that RhFeMnZ is more compressible. The shear modulus (G) quantifies the transverse deformation resistance of a material. Furthermore, the ductility or brittleness of the materials which may be predicted by means of assessing Pugh's ratio (B/G) [33]. The critical point at which the ratio (B/G) becomes 1.75. A material beyond this threshold is classified as ductile, whereas a number below 1.75 indicates brittleness. Based on the compounds analysed, a (B/G) ratio of 1.55745 indicates that IrMnCrGe-Type I is brittle, while the (B/G) values of the other compounds (>1.75) also indicate brittle behaviour. The data shown in Table 3 clearly indicates that the computed values of σ for IrMnCrGe-Type I, IrMnCrSi-Type III, RhFeMnGe-Type III, and RhFeMnSi-Type III are determined to be 0.298, 0.284, 0.311, and 0.294, respectively. This discovery suggests that both materials have the ability to deform without breaking and can be categorised as having central forces and ionic properties. Similarly, the Cauchy's pressure (C_p) is evaluated to determine whether the materials have a brittle or ductile nature. In our compounds, a positive C_p value signifies a ductile behaviour. The anisotropic factor (A_1) of Zener [34] is used to determine with respect to whether the materials exhibit isotropic or anisotropic properties. Complete isotropy is denoted by a value of unity, which suggests that qualities are consistent in all directions. The compounds' obtained (A_1) values surpass unity, providing confirmation of their

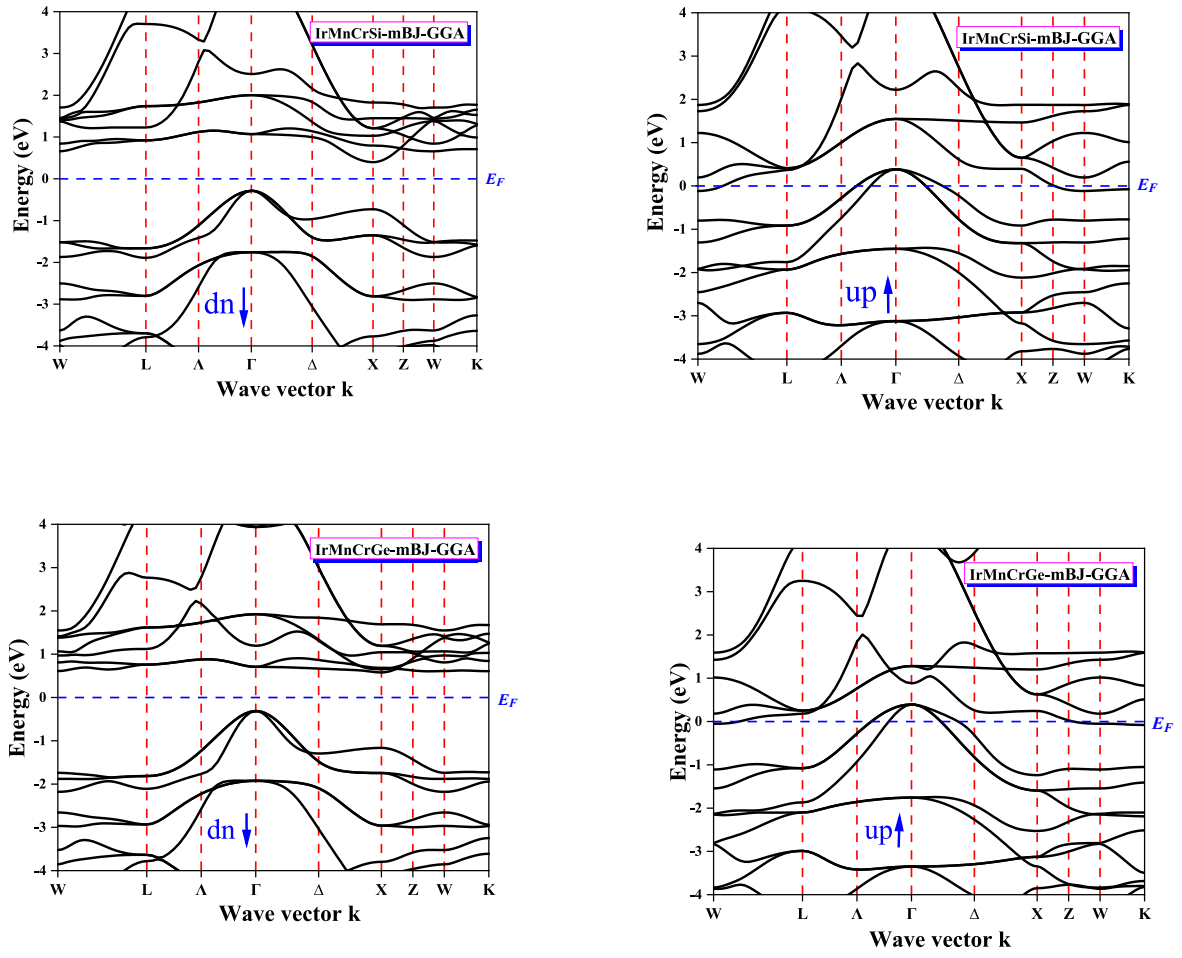

Fig. 4. (*continued*).

Table 4
Energy gap values calculated by the two GGA and mBJ-GGA approximations for the quaternary Heusler compounds RhFeMnZ and IrMnCrZ (where Z = Si, and Ge).

Compounds	The spins	E_g (eV)	
		GGA	mBJ-GGA
RhFeMnSi-Type III	Up	/	/
	Down	0.525	0.957
RhFeMnGe	Up	/	/
Type III	Down	/	0.66
IrMnCrSi	Up	/	/
Type III	Down	0.172	0.745
IrMnCrGe	Up	/	/
Type I	Down	0.228	0.891

anisotropic nature. Moreover, the melting temperature (T_{melt}) values for the compounds IrMnCrGe-Type I, IrMnCrSi-Type III, RhFeMnGe-Type III, and RhFeMnSi-Type III are 2263.4686, 2565.4052, 2372.6819, and 2607.9607, respectively. The values presented here have been computed using the IRELAST method [30], which is a component of the WIEN2k package. Essentially, these documented values provide strong evidence for the practical use of these alloys in various engineering and commercial settings. Moreover, they assert the feasibility of the aforementioned calculations, we have also determined the longitudinal sound velocity, transverse sound velocity, and average sound velocity of the compounds RhFeMnZ and IrMnCrZ (Z = Si, and Ge). The data shown in Table 3 provides proof that elastic longitudinal waves have a higher propagation speed compared to elastic transverse waves. Based on the given sound velocities, the Debye temperature (θ_D) has been computed. The Debye temperatsure is a significant physical parameter that establishes connections between many physical characteristics, including specific heat capacity, thermal conductivity, and melting point of the crystal, in relation to its elastic constants. The Debye temperature (θ_D) can be determined from the temperature dependence of the second-

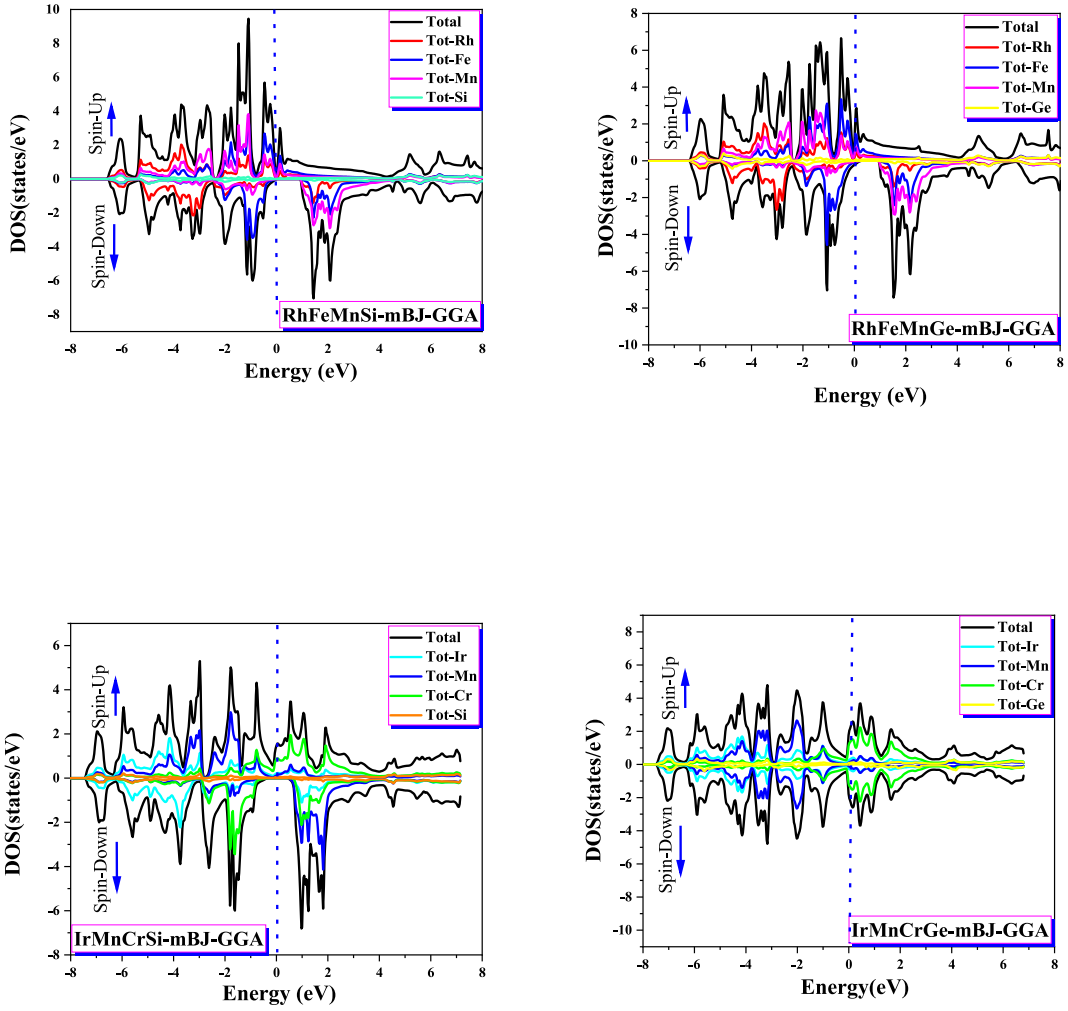

Fig. 5. Total density of states of the RhFeMnZ and IrMnCrZ (where Z = Si; Ge) compounds calculated by mBJ-GGA.

Table 5
Calculated using GGA and mBJ-GGA, the total electron density N(E_F) up and down at the *Fermi* level with *P*-polarisation for RhFeMnZ and IrMnCrZ (where Z = Si, Ge) compounds.

Approximation	GGA			mBJ-GGA		
	N(E_F)		*P*	N(E_F)		*P*
	N(E_F)↓	N(E_F)↑		N(E_F) ↓	N(E_F) ↑	
RhFeMnSi	0	0.06	100 %	0	0.03	100 %
RhFeMnGe	0.05	0.24	65 %	0	0.29	100 %
IrMnCrSi	0	0.56	100 %	0	0.66	100 %
IrMnCrGe	0	1.09	100 %	0	1.37	100 %

order elastic constants at low temperatures.

The existence of crystallographic elastic anisotropy can have a substantial influence on a range of physical phenomena, including but not limited to anisotropic deformation, susceptibility cracking, and elastic instability. The elastic anisotropy of RhFeMnZ and IrMnCrZ (Z = Si, Ge) has been measured utilising three additional distinct methodologies in addition to the initial calculation of the Zener parameter (A_1).

The second method involves the assessment of the extent of elastic anisotropy in shear conditions, as outlined in reference [35]:

$$A_G = (G_V - G_R)/(G_V + G_R) \times 100 \quad (4)$$

For isotropic materials, the A_G value is zero. Anisotropy in elastic shear exists between A_G and zero. At one hundred percent A_G, the utmost potential anisotropy is present. The distinction between IrMnCrGe-Type I, IrMnCrSi-Type III, RhFeMnGe-Type III, RhFeMnSi-Type III is their shear anisotropy A_G. As shown in Table 3, the corresponding percentages for the values are approximately 11.7597, 8.14018, 9.90621, 7.37909, according to the GGA approximation. RhFeMnZ and IrMnCrZ (Z = Si, Ge) materials demonstrate a notable level of anisotropy with respect to their shear modulus.

The third approach entails the computation of the universally recognised index, sometimes referred to as the universal index [36].

$$A^U = 5\frac{G_V}{G_R} + \frac{B_V}{B_R} - 6 \quad (5)$$

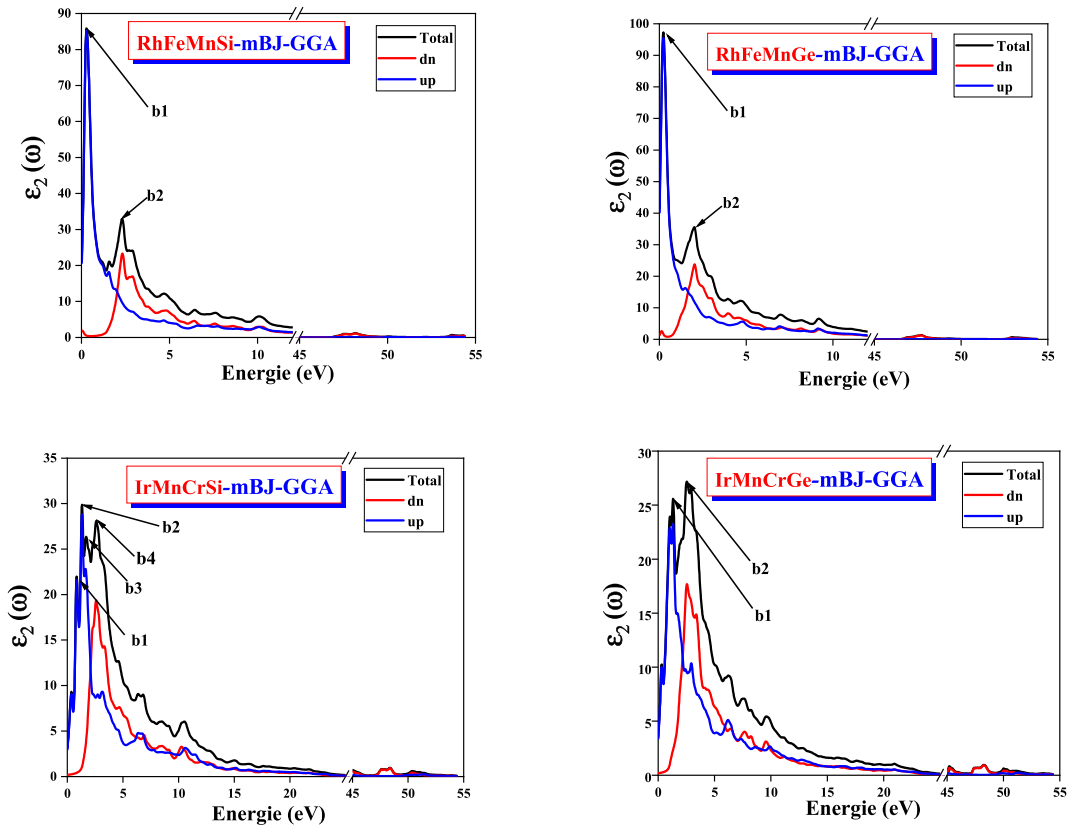

(a)

Fig. 6. Variation of **(a)** and **(b)**, ε_2 (ω) and k(ω), **(c)** and **(d)**, ε_1 (ω) and n(ω), **(e)** and **(f)**, R(ω), and I(ω), **(g)** and **(h)** σ(ω) and L(ω) as a function of energy for RhFeMnZ and IrMnCrZ (where Z = Si; Ge) compounds calculated by mBJ-GGA.

A^U values for isotropic materials are zero. A transition occurs in which the amplitude of crystallographic anisotropy becomes positive from zero. The results shown in Table 3 illustrate the universal index A^U that was computed using the GGA approximation for IrMnCrGe-Type I, IrMnCrSi-Type III, RhFeMnGe-Type III, RhFeMnSi-Type III. The A^U values obtained are approximately 1.33268, 0.886152, 1.09954, 0.796698, correspondingly. Each compound demonstrates substantial elastic anisotropy.

For useful purposes, it is preferable to employ surface structures that exhibit the directional reciprocal of Young's modulus. Polar diagrams in three dimensions can be used to represent the distribution of the E modulus for a cubic system, as follows [37]:

$$E = \frac{1}{S_{11} - 2\left(S_{11} - S_{12} - \frac{1}{2}S_{44}\right)\left(n_1^2 n_2^2 + n_2^2 n_3^2 + n_3^2 n_1^2\right)} \tag{6}$$

In terms of spherical coordinates, the directions along the x, y, and z axes correspond to the cosines $n_1 = \sin\theta\cos\varphi$, $n_2 = \sin\theta\sin\varphi$, and $n_3 = \cos\theta$, where S_{ij} is the deformability elastic constant. Fig. 3 illustrates the modulus of Young for RhFeMnZ (Z = Si, Ge) and IrMnCrZ (Z = Si, Ge) in relation to the projected orientation, with the elastic compliance factors serving as a benchmark. A three-dimensional closed surface is generated by the solution to Eq. (6), and Young's modulus in the specified direction is equal to the distance between the surface and the origin of the corresponding coordinate system. This surface would have the appearance of a sphere if the underpinning structure were entirely isotropic. Clearly, the Young's modulus surfaces of RhFeMnZ and IrMnCrZ (Z = Si, Ge) do not have a spherical morphology. As a result of the unique bonding properties possessed by adjacent atomic planes, these two compounds demonstrate a significant degree of anisotropy. Consequently, a considerable separation exists among the atomic planes. For the RhFeMnZ and IrMnCrZ (Z = Si, Ge) materials, elastic anisotropy is greater in the (X = Y) plane than in the (XY), (XZ), and (YZ) planes.

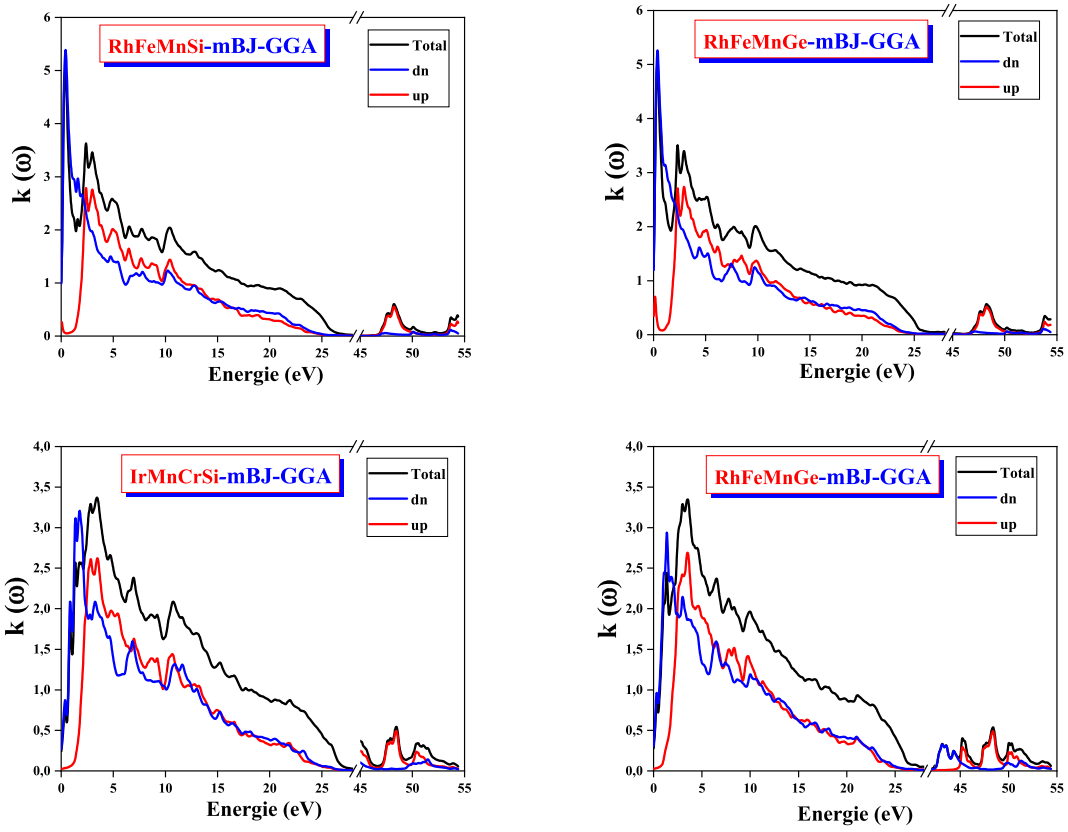

(b)

Fig. 6. (*continued*).

3.3. Electronic band structure and density of states

We calculated the energy bands for the four compounds RhFeMnZ and IrMnCrZ (Z = Si, Ge) and injected the structural parameters found previously by approximating the most stable type with the GGA. Calculations were performed on the spin-polarized bands along the high-symmetry directions of the first *Brillouin* zone for the quaternary Heusler compounds RhFeMnSi, RhFeMnGe, and IrMnCrSi type III and type I for the compound IrMnCrGe using the GGA and mBJ-GGA methods. They are shown in Fig. 4. The alloys of RhFeMnZ and IrMnCrZ (Z = Si, Ge) have been observed to display semi-metallic characteristics. This is clear from Fig. 4, where both the GGA and mBJ-GGA approximations show that the bands of the majority spins cross the *Fermi* energy level, which means the material is metallic. Conversely, the band structure of the minority spins demonstrates a semiconducting nature. Except for the RhFeMnGe compound, which represents a metallic nature with the GGA approximation. In the case of minority spins, the valence band maximum (VBM) and conduction band minimum (CBM) are positioned at the Γ and X high symmetry points, respectively. In *p*-type semiconductors, the *Fermi* energy is near the VBM, except for the IrMnCrGe compound, where it is close to the CBM, making it an *n*-type semiconductor. Thus, in the minority spin channel and employing the mBJ-GGA approximation, the quaternary Heusler compounds RhFeMnSi, RhFeMnGe, IrMnCrSi, and IrMnCrGe exhibit an indirect bandgap of 0.957 eV, 0.66 eV, 0.745 eV, and 0.891 eV, respectively, as shown in Table 4. We can conclude that our materials are half-metals using the mBJ-GGA approximation.

To determine the nature of the electronic band structure, we calculated the total density of states TDOS and partial density of states PDOS of the quaternary compounds RhFeMnZ and IrMnCrZ (Z = Si, Ge) with the GGA and mBJ-GGA approximations. The total and partial densities of states of the RhFeMnSi, RhFeMnGe, and IrMnCrSi compounds of type III and type I for the IrMnCrGe compound calculated by GGA and mBJ-GGA are shown in Fig. 5.

For quaternary compounds RhFeMnZ (Z = Si, Ge), below the *Fermi* level, Fe, Mn, and Rh atoms have a majority contribution in the TDOS of majority spins due to *3d*- and *4d*-layer electrons, respectively, and for minority spins, Fe and Rh atoms have a majority contribution in the

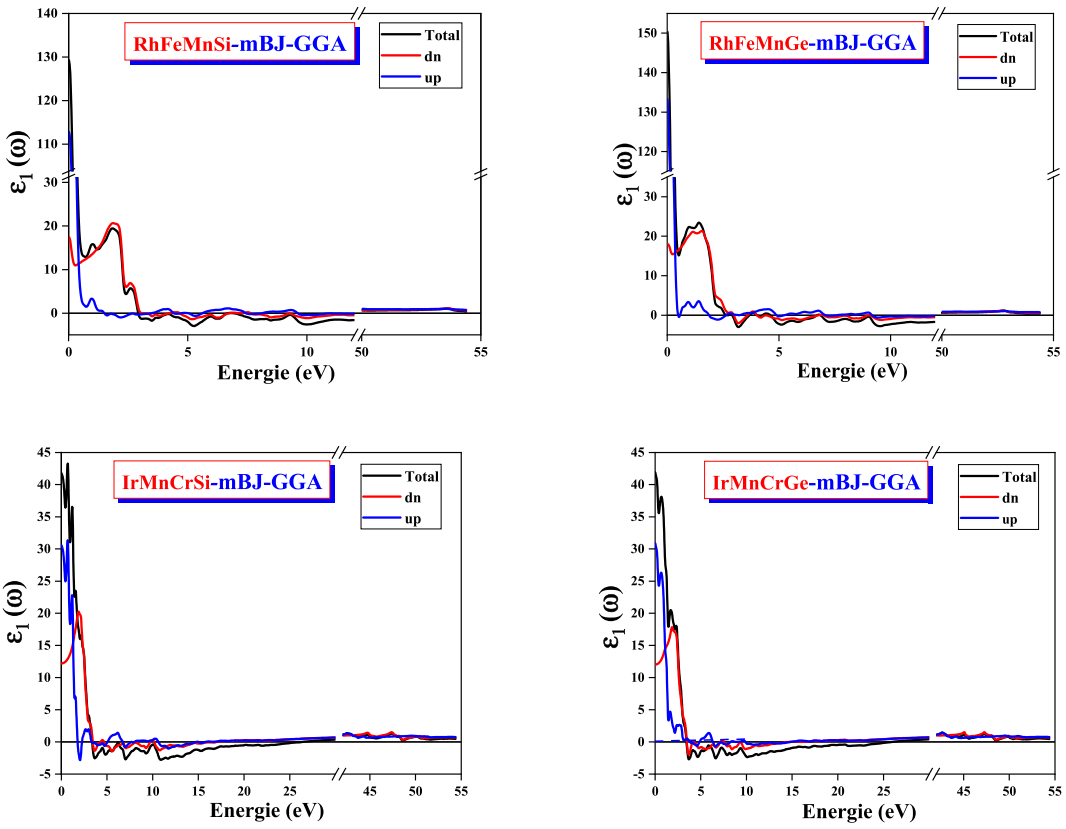

(c)

Fig. 6. (*continued*).

TDOS due to *3d*- and *4d*-layer electrons, respectively. For IrMnCrZ compounds (Z = Si, Ge), below the *Fermi* level, Mn and Ir atoms have a majority contribution in the TDOS of majority spins; this contribution is due to 3d-Mn and 5d-Ir electrons, respectively, while Ir and Cr atoms have a dominant contribution below the *Fermi* level for minority spins due to *5d*-Ir and *3d*-Cr layer electrons, respectively. As far as the conduction band is concerned, our compounds have a mixed contribution from the d-orbitals of the X, X_0, and Y atoms, and the contribution from the Z atom is neglected.

3.4. Magnetic properties

In order to verify the presence of the energy gap, we computed the overall density at the Fermi level, in conjunction with the spin polarization, which provides insight into the material's characteristics through the following correlation:

$$P = \frac{N(E_F)\uparrow - N(E_F)\downarrow}{N(E_F)\uparrow + N(E_F)\downarrow} \quad (7)$$

Due to their high electron spin polarization, the quaternary Heusler compounds RhFeMnZ and IrMnCrZ (Z = Si, Ge) are regarded as prospective materials for spintronic applications. Eq. (7) was utilized to calculate electron spin polarization at *Fermi* energy; this is a standard method for determining spin polarization in solids. The polarization of the electron spin of the materials RhFeMnZ and IrMnCrY (Z = Si, Ge) was found to be 100 % using the mBJ-GGA method (refer to Table 5 for details). The ferromagnetic nature of the quaternary Heusler compounds RhFeMnGe-Type III, IrMnCrSi-Type III, and IrMnCrGe-Type I is further validated by the density of states under both the mBJ-GGA and GGA approximations. This indicates that these compounds have the potential to serve as viable materials for forthcoming spintronic applications.

RhFeMnZ (Z = Si, Ge) compounds are ferromagnetic and have a total magnetic moment of 4 μ_B. On the other hand, IrMnCrZ (Z = Si, Ge) compounds are ferrimagnetic and have a total magnetic moment of 2 μ_B. The main contribution to the total magnetic moment of the quaternary Heusler compounds RhFeMnZ and IrMnCrZ (Z = Si, Ge) originates from the local magnetic moments of the manganese (Mn) atoms. Silicon (Si)

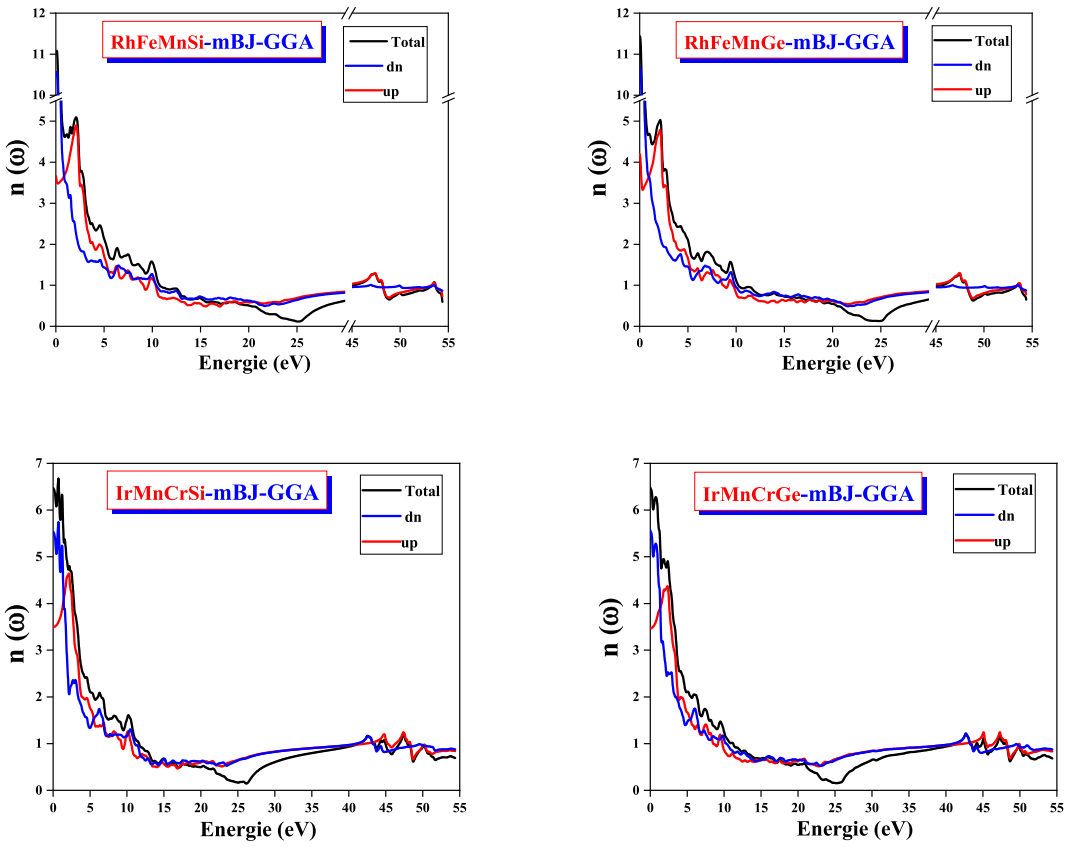

(d)

Fig. 6. (*continued*).

and germanium (Ge) atoms make a negligible contribution to the total magnetic moment.

Undoubtedly, among the most intriguing characteristics of Heusler compounds is the Slater-Pauling rule, which establishes a correlation between the total number of valence electrons (N_v) and the compound's total spin magnetic moment (M_{Tot}). Heusler compounds consisting of perfect semi-metallic ferromagnets and spin-gap-free semiconductors adhere rigorously to this principle, owing to the integer value of their total spin magnetic moment. Since valence electrons in all Heusler compounds are capable of existing in either high-spin or low-spin states, the total spin magnetic moment is determined by the discrepancy in their numbers. Frequently, a complex Slater-Pauling rule results from the relative position of the d states of atoms Y in quaternary Heusler compounds with regard to X and X_0. Each compound adheres to the subsequent principle:

$$M_{Tot} = (N_v - 24)\mu_\beta \quad (8)$$

The total magnetic moment in the stable structure of every compound is an integer, which is an essential requirement for the compounds to qualify as semi-metallic.

3.5. Optical behavior

The examination of the optical properties of solids has become a highly effective method for understanding the electronic characteristics of substances. Fig. 6(a) demonstrates that the spectra of the imaginary part ε_2 (ω) of the four half-metals exhibit nearly identical behavior. The optical absorption edge serves as the primary determinant for distinguishing the boundary between the valence (VB) and conduction (CB) bands. This calculation will provide the threshold energy required for the indirect optical transition from the upper valence band V1 to the lower conduction band C1 (V1 → C1 transition). The band numbering is based on the bottom of the conduction band and the top of the valence band. Also referred to as the primary absorption threshold.

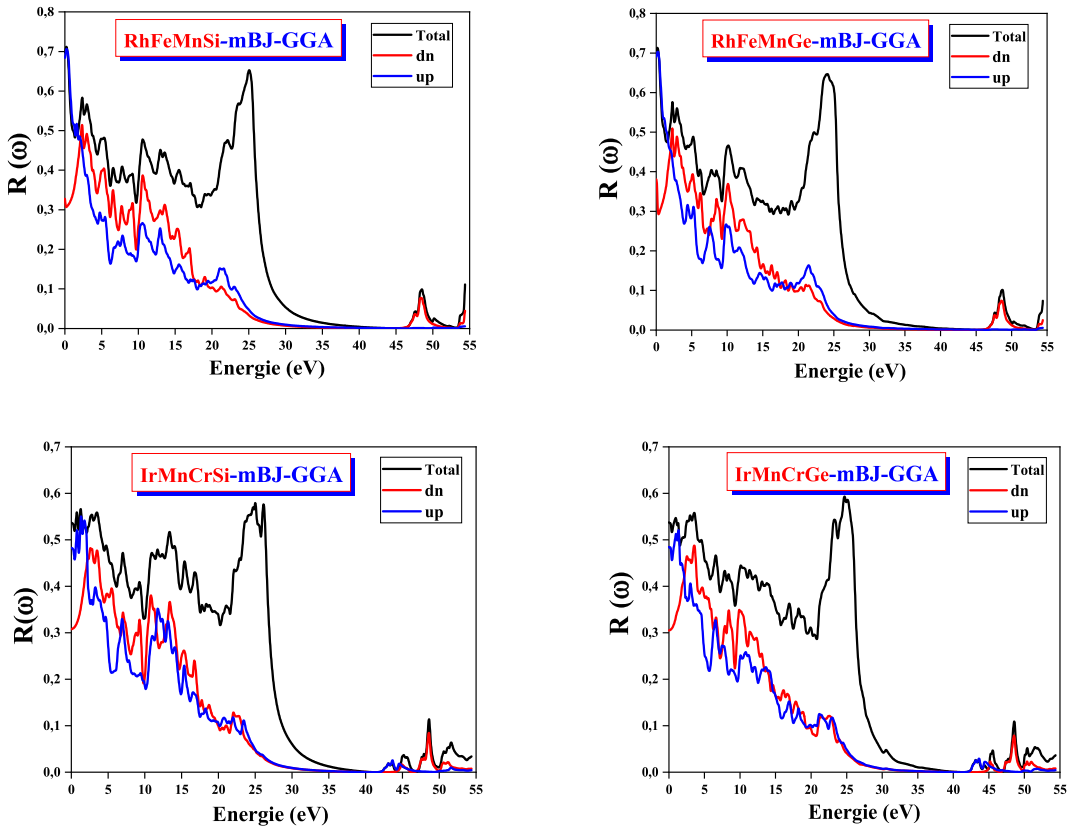

(e)

Fig. 6. (*continued*).

We have identified two primary absorption peaks, denoted as b1 and b2, situated at specific energy levels: 0.2610 eV and 2.2765 eV for RhFeMnSi, 0.31293 eV and 2.68032 eV for RhFeMnGe, 0.3197 eV and 2.5442 eV for IrMnCrGe. The fourth compound, IrMnCrSi, has four distinct peaks labeled as b1, b2, b3, and b4. These peaks are placed at energies of 0.8299 eV, 1.3197 eV, 1.7007 eV, and 2.6531 eV, respectively. Every compound has b1 peaks in the infrared range. The remaining peaks, b2, b3, and b4, are part of the visible spectrum. The peaks observed are a result of electronic transitions in the majority state of b1 and the minority states of b2, with the exception of IrMnCrSi. In IrMnCrSi, the peaks are due to electronic transitions in the majority state for both b1 and b2. Peak b3 is a result of mixed electronic transitions involving both the majority and minority states. Peak b4 is solely due to minority electronic transitions. In the minority state, the dielectric function of RhFeMnSi, RhFeMnGe, IrMnCrSi, and IrMnCrGe reaches its highest absorption point at energies of 2.3264 eV, 2.8708 eV, 2.5986 eV, and 2.5442 eV, respectively. In the majority state, the highest absorption point occurs at energies of 0.1276 eV, 0.2857 eV, 1.3197 eV, and 1.0497 eV, respectively. The order of optical absorption for the four compounds is as follows. The energy levels of the spectra of the four compounds decrease in the following order: RhFeMnGe, IrMnCrSi, IrMnCrGe, and RhFeMnSi. The decrease in bandgap can be observed in the following order: RhFeMnSi, IrMnCrGe, IrMnCrSi, and RhFeMnGe.

Fig. 6(b) illustrates the spectrum of variation in the extinction coefficient k(ω). Maximum extinction coefficient values of 0.4217 eV and 0.3945 eV correspond to energies in the infrared region for RhFeMnSi and RhFeMnGe, respectively, which are associated with the minority states' interband transitions; for IrMnCrSi and IrMnCrGe, these values are attributed to the majority states' interband transitions in the visible region, and are 3.4422 eV and 3.5510 eV, respectively. Once the photon energies surpass this peak, the extinction coefficient for every compound gradually decreases.

Fig. 6(c) displays the computed outcomes for the real (dispersive) component ε_1 (ω) of the dielectric function of the quaternary Heusler compounds RhFeMnSi, RhFeMnGe, IrMnCrSi, and IrMnCrGe. The absence of scattering is indicated by a zero-crossing of the spectra. It is

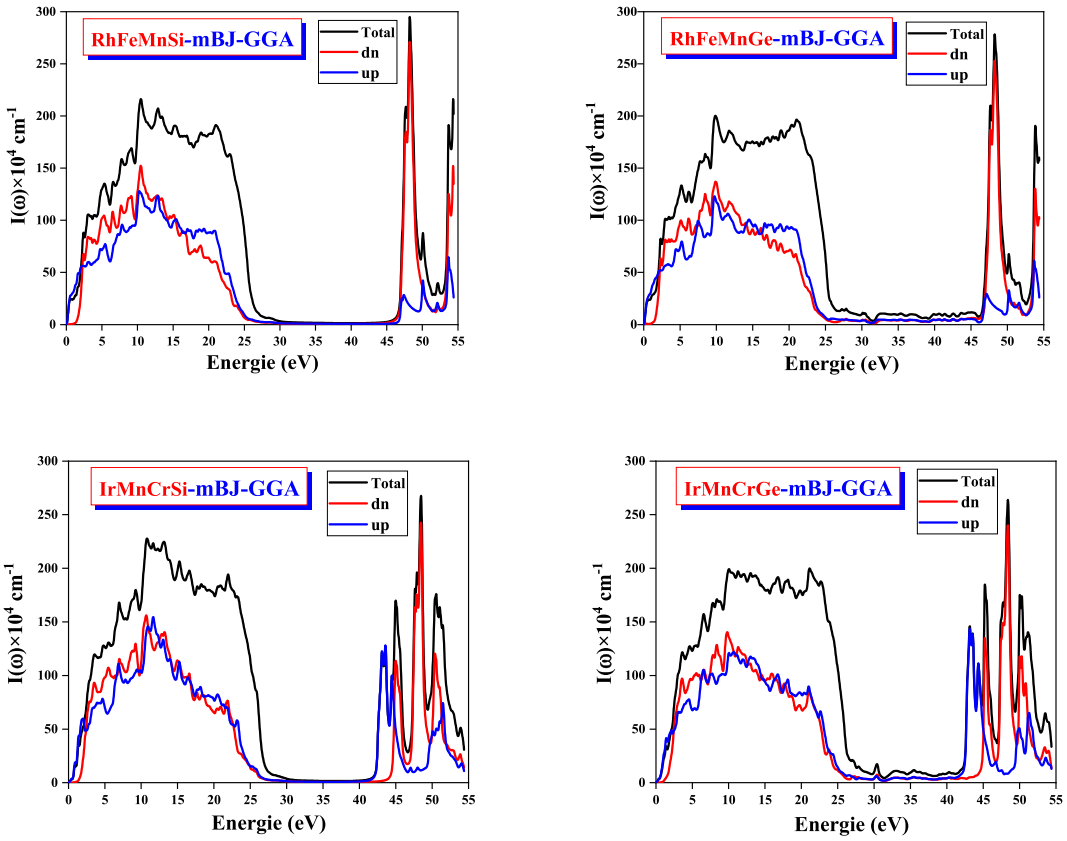

(f)

Fig. 6. (*continued*).

seen that for all of these compounds, the function reaches a value of zero, indicating that scattering at these energy levels is absent and, as a result, absorption is at its highest level. The real component of the values drops as the photon energy increases and eventually reaches zero. Following a minimum, the dispersive component returns to zero. The primary peaks derived from mBJ-GGA computations are situated within the infrared spectrum. The real part of the dielectric function reaches zero at energies of 2.7650 eV, 2.6803 eV, 1.7007 eV, and 2.5424 eV for the materials RhFeMnSi, RhFeMnGe, IrMnCrSi, and IrMnCrGe, respectively see Table 7. The primary peak is succeeded by a fluctuating pattern centered around zero, after which the spectrum turns negative. It reaches a minimum and then gradually returns to zero at approximately 24.6467 eV, 25.2999 eV, 26.4086 eV, and 26.0004 eV for RhFeMnSi, RhFeMnGe, IrMnCrSi, and IrMnCrGe, respectively. The peak with the maximum intensity is detected in the RhFeMnGe compound, followed by RhFeMnSi, IrMnCrGe, and finally IrMnCrSi.

Fig. 6(d) illustrates the Refractive index $n(\omega)$, which typically mirrors the geometry of the real part. The materials RhFeMnSi, RhFeMnGe, IrMnCrSi, and IrMnCrGe have zero-frequency refractive indices of 11.4374, 11.0410, 6.48040, and 6.46929, respectively. These values were obtained using the mBJ-GGA approximation. Thus, it may be inferred that RhFeMnSi possesses the highest refractive index value. The refractive index falls as the frequency increases until reaching 25 eV, at which point it starts to steadily increase. Additionally, it demonstrates non-linear characteristics. The computed static refractive index is presented in Table 6. As far as we know, there is no existing empirical or theoretical information that may be used for comparison.

Fig. 6(e) shows the variation in reflectivity R(ω) of our compounds. The reflectivity started at 68.38 %, 69.02 %, 48.26 %, and 48.47 % for the minority spin channel and at 32.77 %, 38.09 %, 30.78 %, and 30.51 % for the majority states, leading to a total reflectivity of 69.75 %, 70.71 %, 53.66 %, and 53.73 % for RhFeMnSi, RhFeMnGe, IrMnCrSi, and IrMnCrGe, respectively. The main peak is at an energy of 0.2313 eV, 0.1768 eV, 24.9936 eV, and 24.6943 eV for RhFeMnSi, RhFeMnGe, IrMnCrSi, and IrMnCrGe, respectively. We note that the RhFeMnSi compound has the highest reflectivity, followed by RhFeMnGe, then

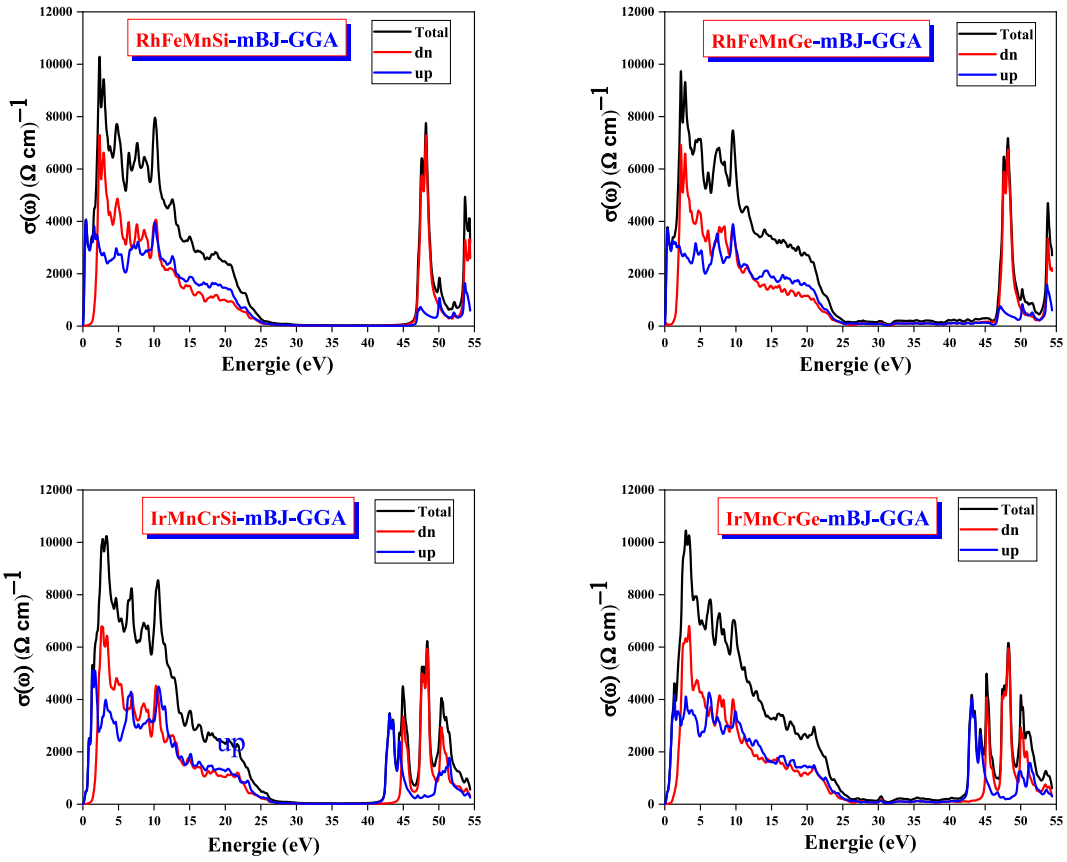

(g)

Fig. 6. (*continued*).

IrMnCrGe, and finally IrMnCrSi.

Fig. 6(f) illustrates the relationship between the total absorption coefficient I(ω) and the energy of the photons for the investigated Heusler quaternary compounds. At low energies, the function I(ω) exhibits a quick increase in the vicinity of the near ultraviolet region, followed by a subsequent decline. It then experiences another increase, reaching a second peak, before decreasing once again. Finally, there is a third increase leading to a third peak, both of which are located in the far ultraviolet region. The peaks observed in the electronic band spectrum are generated by interband and intraband transitions occurring between different high symmetries. It was observed that the compounds exhibit their maximum absorption peaks in the ultraviolet region. Subsequently, these compounds exhibit a strong capacity to absorb the low and mid UV range, as depicted in Fig. 6(f). The absorption spectra of RhFeMnSi show peaks in the energy range of 2.9178–24.7759 eV and 47.1337–54.3547 eV. For RhFeMnGe, the absorption spectra suggest peaks in the energy range of 4.5579–23.9424 eV and 47.3886–54.3819 eV. The absorption spectra of IrMnCrSi show peaks in the energy range of 3.4694–24.2392 eV and 43.0620–51.7152 eV. For IrMnCrGe, the absorption spectra indicate peaks in the energy range of 3.3878–24.7872 eV and 42.9258–51.6336 eV. The absorption coefficient is highest for RhFeMnSi at an energy of 48.2322 eV, followed by RhFeMnGe at 48.2594 eV, IrMnCrSi at 48.4771 eV, and finally IrMnCrGe at 48.3954 eV. Due to the wide absorption range of our compounds, they exhibit significant intensity. Hence, it may be inferred that our compounds possess the potential to serve as optoelectronic devices.

Fig. 6(g) displays the optical conductivity spectrum, which exhibits many peaks that correspond to transitions between bands. The primary optical conductivity peaks for RhFeMnSi, RhFeMnGe, IrMnCrSi, and IrMnCrGe are located at 2.3265 eV, 2.2721 eV, 3.3334 eV, and 2.9524 eV, respectively. These peaks fall inside the visible part of the electromagnetic spectrum.

Significant values for energy loss in the region spanning from 25.1569 eV to 26.2181 eV are observed in RhFeMnSi, as illustrated in Fig. 6(h). An energy of 25.6467 eV corresponds to the intense apex. RhFeMnGe exhibits a notable energy loss throughout its energy spectrum of 24.8031–25.7011 eV. At 25.2999 eV, the maximum peak occurs. For IrMnCrSi (IrMnCrGe), the maximal energy is measured to be 26.4086 eV (26.0004 eV). The IrMnCrSi (IrMnCrGe) energy loss spectra exhibit noteworthy values within the energy range of 25.1841–26.5447 eV. The plasma frequency ω_p is the average peak of the energy loss function. Therefore, as an example, the plasma energy $\hbar\omega_p$ of its peak position is 24.6467 eV, 25.2999 eV, 26.4086 eV and 26.0004 eV for RhFeMnSi, RhFeMnGe, IrMnCrSi, and IrMnCrGe respectively. Then, the plasma frequency ω_p is 3.7445×10^{16} s^{-1}, 3.8437×10^{16} s^{-1}, 4.0122×10^{16} s^{-1} and 3.9502×10^{16} s^{-1} for the quaternary Heusler compounds RhFeMnSi, RhFeMnGe, IrMnCrSi, and IrMnCrGe respectively.

4. Conclusion

Here we have reported the electronic structure, magnetism, mechanical, and optical properties of RhFeMnSi, RhFeMnGe, IrMnCrSi, and IrMnCrGe by using WIEN2k computational code. The present study involved calculating the spin-polarized band structure for various quaternary Heusler compounds, namely RhFeMnSi, RhFeMnGe, IrMnCrSi type III, and IrMnCrGe type I. The compounds RhFeMnZ and IrMnCrZ

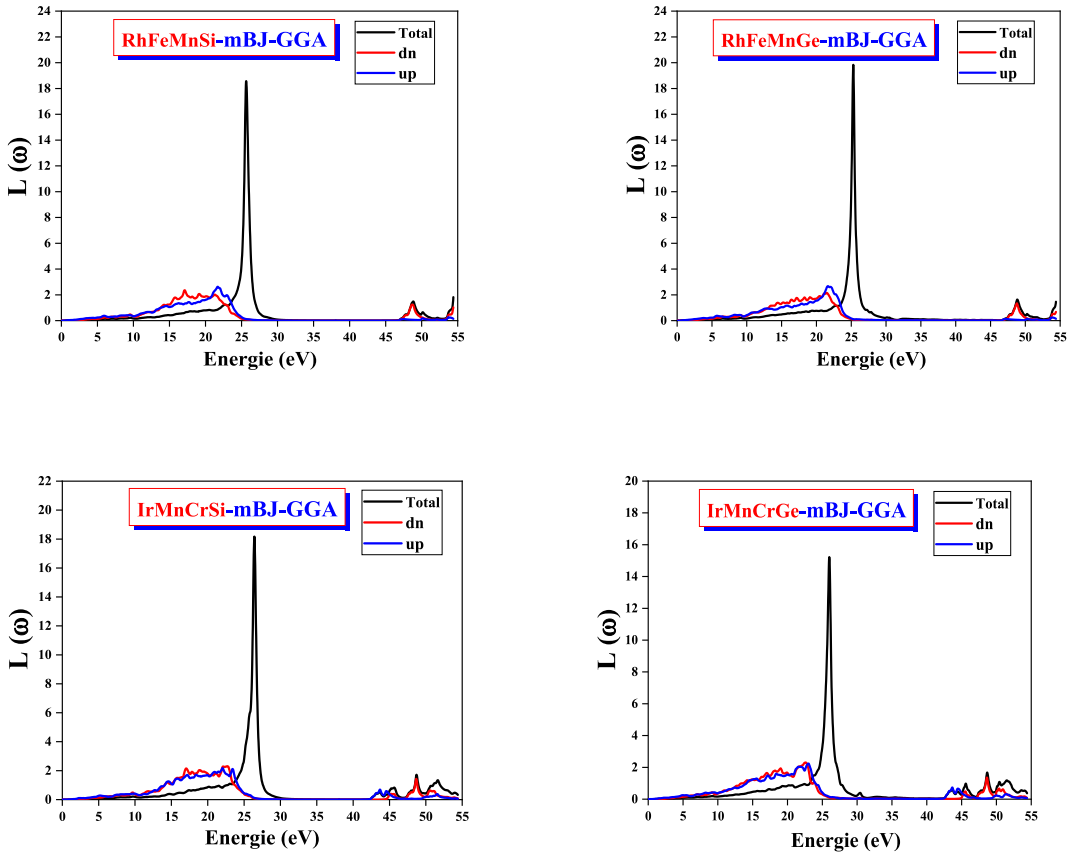

(h)

Fig. 6. (*continued*).

Table 7
ε_1 (0) and n (0) for the compounds RhFeMnZ and IrMnCrY (where Z = Si, Ge) calculated using the approximations GGA and mBJ-GGA.

Alloys	ε_1 (0)			n (0)		
	Spins	GGA	mBJ-GGA	Spins	GGA	mBJ-GGA
RhFeMnSi	Up	118.358	108.534	Up	10.9498	10.4649
	Down	15.0531	13.3245	Down	3.88010	3.65903
	Total	132.411	120.859	Total	11.5683	11.0410
RhFeMnGe	Up	133.290	112.793	Up	11.6728	10.6875
	Down	18.0230	17.4710	Down	4.24841	4.19413
	Total	150.313	129.264	Total	12.3747	11.4374
IrMnCrSi	Up	27.1787	30.5917	Up	5.21546	5.53748
	Down	15.0750	12.2006	Down	3.88282	3.49303
	Total	41.2537	41.7923	Total	6.42449	6.46929
IrMnCrGe	Up	33.2390	30.8918	Up	5.77351	5.56646
	Down	16.1136	12.0270	Down	4.01440	3.46810
	Total	48.3526	41.9188	Total	6.95920	6.48040

(where Z = Si, Ge) exhibit semi-metallic behavior according to the GGA and mBJ-GGA approximations. This is because the structure of the minority spin bands is semiconducting in nature, whereas the majority spin bands exhibit metallic behaviour by crossing the Fermi energy level. Apart from the RhFeMnGe compound, which demonstrates metallic characteristics when the GGA approximation is implemented. The quaternary Heusler compounds RhFeMnSi, RhFeMnGe, IrMnCrSi, and IrMnCrGe exhibit indirect band gaps of 0.957 eV, 0.66 eV, 0.745 eV, and 0.891 eV, respectively, when analyzed in the minority spin channel and using the mBJ-GGA approximation. RhFeMnZ (Z = Si, Ge) compounds are ferromagnetic and have a total magnetic moment of 4 μ_B. On the other hand, IrMnCrZ (Z = Si, Ge) compounds are ferrimagnetic and have a total magnetic moment of 2 μ_B. This study presents the optical characteristics of the quaternary Heusler compounds RhFeMnZ and IrMnCrZ

Table 6
The total magnetic moment and partial magnetic moment of the compounds RhFeMnZ and IrMnCrY (where Z = Si, Ge) calculated using the approximations GGA and mBJ-GGA.

The compounds	*The moment m_O (μ_B /f. u)*	Our calculations		Other calculations [21]
		GGA	mBJ-GGA	
RhFeMnSi	m_O (*Interstitial*)	0.01435	−0.15181	/
	m_O (Rh) (μ_β /ato)	0.27736	0.21992	0.29
	m_O (Fe) (μ_β /atom)	0.82163	0.91756	0.85
	m_O (Mn) (μ_β /atom)	2.89530	3.02453	2.95
	m_O (Si) (μ_β /atom)	−0.02311	−0.04750	−0.05
	m_O (Tot) (μ_β /atom)	4.00396	4.00054	4.01
RhFeMnGe	m_O (*Interstitial*)	0.01435	−0.15181	/
	m_O (Rh) (μ_β /atom)	0.27736	0.21992	0.26
	m_O (Fe) (μ_β /atom)	0.80159	0.91304	0.80
	m_O (Mn) (μ_β /atom)	2.95640	3.13221	3.05
	m_O (Ge) (μ_β /atom)	−0.03058	−0.06317	−0.05
	m_O (Tot) (μ_β /atom)	4.01912	4.05019	4.07
IrMnCrSi	m_O (*Interstitial*)	0.04583	−0.01761	/
	m_O (Ir) (μ_β /atom)	0.18455	0.21043	0.20
	m_O (Mn) (μ_β /atom)	2.77456	3.04083	3.00
	m_O (Cr) (μ_β /atom)	−1.00184	−1.25871	−1.26
	m_O (Si) (μ_β /atom)	0.02202	0.02524	0.03
	m_O (Tot) (μ_β /atom)	2.02511	2.00018	2.00
IrMnCrGe	m_O (*Interstitial*)	0.05354	−0.02771	/
	m_O (Ir) (μ_β /atom)	0.21788	0.24943	0.24
	m_O (Mn) (μ_β /atom)	2.98500	3.31372	3.22
	m_O (Cr) (μ_β /atom)	−1.28169	−1.57838	−1.54
	m_O (Ge) (μ_β /atom)	0.04126	0.04309	0.04
	m_O (Tot) (μ_β /atom)	2.01600	2.00016	2.00

(where Z represents Si or Ge). This study presents and analyzes general models of the optical parameters, comprising both the real and imaginary parts of the dielectric constant, absorption coefficients, and the refractive index. The results indicate minimal energy differences between these parameters. $\varepsilon_1(0)$) and $n(0)$ show an increasing trend from IrMnCrGe to IrMnCrSi, then to RhFeMnSi, and finally to RhFeMnGe. The compounds RhFeMnZ and IrMnCrZ (Z = Si, Ge) display absorption in the ultraviolet (UV) spectrum, rendering them favorable choices for utilization in UV photodetectors, ultraviolet (UV) emitting devices, and power electronic devices. This is a result of their inherent absorption limitations and the existence of the most intense absorption peaks.

CRediT authorship contribution statement

H. Baaziz: Writing – review & editing, Writing – original draft, Visualization, Validation, Supervision, Methodology. **T. Ghellab:** Investigation, Formal analysis, Data curation, Conceptualization. **Z. Charifi:** .

Declaration of competing interest

The authors declare that they have no known competing financial interests or personal relationships that could have appeared to influence the work reported in this paper.

Data availability

Data will be made available on request.

Acknowledgments

The authors (H. Baaziz, T. Ghellab, and Z. Charifi) would like to thank the general directorate for scientific research and technological development for their financial support during the realization of this work.

References

[1] R.A. de Groot, F.M. Mueller, P.G. Van Engen, K.H.J. Buschow, Phy. Rev. Lett. 50 (1983) 2024.
[2] I. Zutic, J. Fabian, S.D. Sharma, Rev. Mod. Phys. 76 (2004) 323.
[3] Z.H. Xiong, D. Wu, Z.V. Vardeny, J. Shi, Nature 427 (2004) 821.
[4] J. Han, G. Gao, Appl. Phys. Lett. 113 (2018) 102402.
[5] D. Kurebayashi, K. Nomura, Sci. Rep. 9 (2019) 5365.
[6] M.E. Jamer, Y.J. Wang, G.M. Stephen, I.J. McDonald, A.J. Grutter, G.E. Sterbinsky, D.A. Arena, Phys. Rev. Appl. 7 (2017) 064036.
[7] L. Bainsla, K.Z. Suzuki, M. Tsujikawa, H. Tsuchiura, M. Shirai, S. Mizukami, Appl. Phys. Lett. 112 (2018) 052403.
[8] M.I. Khan, H. Arshad, M. Rizwan, S.S.A. Gillani, M. Zafar, S. Ahmed, M. Shakil, J. Alloys Compd. 819 (2020) 152964.
[9] C. Felser, I. Wollmann, S. Chadov, G.H. Fecher, S.S. Parkin, APL Mater. 3 (2015) 041518.
[10] P.J. Brown, K.U. Neumann, P.J. Webster, K.R.A. Ziebeck, J. Phys. Condens. Matter 12 (2000) 1827.
[11] T. Graf, C. Felser, S.S. Parkin, Prog. Solid State Ch. 39 (2011) 1.
[12] P. Klaer, B. Balke, V. Alijani, J. Winterlik, G.H. Fecher, C. Felser, H.J. Elmers, Phys. Rev. B 84 (2011) 144413.
[13] G.Y. Gao, L. Hu, K.L. Yao, B. Luo, N. Liu, J. Alloys Compd. 551 (2013) 539.
[14] S. Berri, D. Maouche, M. Ibrir, F. Zerarga, J. Magn. Magn. Matter. 378 (2015) 7.
[15] Q. Gao, H.H. Xie, X.R. Hu, Superlattices Microstruct. 85 (2015) 536.
[16] X. Wang, Z. Cheng, J.L. Wang, X.L. Wang, G. Liu, J. Mater. Chem. C 4 (2016) 7176.
[17] P. Wang, J.B. Xia, H.B. Wu, J. Magn. Magn. Matter. 490 (2019) 165490.
[18] Y. Jin, P. Kharel, P. Lukashev, S. Valloppilly, B. Staten, J. Herran, I. Tutic, M. Mitrakumar, B. Bhusal, A.O. Connell, K. Yang, Y. Huh, R. Skomski, D.J. Sellmyer, J. Appl. Phys. 120 (2016) 053903.
[19] L. Bainsla, K.G. Suresh, A.K. Nigam, M.R. Manivel, B.C. Varaprasad, Y. K. Takahashi, K. Hono, J. Appl. Phys. 116 (2014) 203902.
[20] L. Bainsla, A.I. Mallick, A.A. Coelho, A.K. Nigam, B.C.S. Varaprasad, Y. K. Takahashi, A. Alam, K.G. Suresh, K. Hono, J. Magn. Magn. Matter. 394 (2015) 82.
[21] S. Nepal, R. Dhakal, I. Galanakis, S.M. Winter, R.P. Adhikari, and G, C. Kaphle *Phys. Rev. Materials* 6 (2022) 114407.
[22] P. Blaha, K. Schwarz, P. Sorantin, Tricky, Comput. Phys. Commun. 59 (1990) 399–415.
[23] K. Schwarz, P. Blaha, G.K.H. Madsen, Comput. Phys. Commun. 147 (2002) 71–76.
[24] P. Blaha, K. Schwarz, G.K.H. Madsen, D. Kuasnicke, J. Luitz, Introduction to WIEN2K, an Augmented Plane Wane Plus Local Orbitals Program for Calculating Crystal Properties, Vienna university of technology, Vienna, Austria, 2001.
[25] S. Sanvito, C. Oses, J. Xue, A. Tiwari, M. Zic, T. Archer, P. Tozman, M. Venkatesan, M. Coey, S. Curtarolo, Sci. Adv. 3 (2017) e1602241.
[26] P. Perdew, K. Burke, M. Ernzerhof, Phys. Rev. Lett. 77 (1996) 3865.
[27] F.D. Murnaghan, Proc. Natl. Acad. Sci. USA 30 (1944) 244.
[28] T. Charpin, A Package for Calculating elastic tensors of cubic phases using WIEN, Laboratory of Geometrix F-75252, France, Paris, 2001.
[29] V. Alijani, Winterlik J, Fecher G H, S. S. Naghavi and C. Felser, *Phys. Rev. B* 83 (2011) 184428.
[30] M. Jamal, Cubic-Elastic, 2019. http://www.WIEN2k.at/reg_user/unsupported/cubic-elast/.
[31] S.A. Khandy, S. Yousuf, D.C. Gupta, Phys. Status Solidi B 256 (2019) 1800625.
[32] K. Benkaddour, A. Chahed, A. Amar, H. Rozale, A. Lakdja, O. Benhelal, A. Sayede, J. Alloys Compd. 687 (2016) 211–220.
[33] S.F. Pugh, London, Edinburgh Dublin Philos, Mag. J. Sci. 45 (1954) 823.
[34] S.A. Khandy, D.C. Gupta, Mater. Sci. Eng., B 265 (2021) 114985.
[35] P. Ravindran, L. Fast, P.A. Korzhavyi, B. Johansson, J. Appl. Phys. 84 (1998) 4891.
[36] S.I. Ranganathan, M. Ostoja-Starzewski, Phys. Rev. Lett. 101 (2008) 55504.
[37] J.F. Nye, *Properties of Crystals*, (*Oxford U.*